Title

Catestatin Inhibits Obesity-Induced Macrophage Infiltration and Inflammation in the Liver and Suppresses Hepatic Glucose Production, Leading to Improved Insulin Sensitivity.

Journal

Diabetes, 67(5)

ISSN

0012-1797

Authors

Ying, Wei
Mahata, Sumana
Bandyopadhyay, Gautam K
et al.

Publication Date

2018-05-01

DOI

10.2337/db17-0788

Peer reviewed

Catestatin Inhibits Obesity-Induced Macrophage Infiltration and Inflammation in the Liver and Suppresses Hepatic Glucose Production, Leading to Improved Insulin Sensitivity

Wei Ying,[1] Sumana Mahata,[2] Gautam K. Bandyopadhyay,[1] Zhenqi Zhou,[3] Joshua Wollam,[1] Jessica Vu,[1] Rafael Mayoral,[1] Nai-Wen Chi,[1,4] Nicholas J.G. Webster,[1,4] Angelo Corti,[5] and Sushil K. Mahata[1,4]

Diabetes 2018;67:841–848 | https://doi.org/10.2337/db17-0788

The activation of Kupffer cells (KCs) and monocyte-derived recruited macrophages (McMΦs) in the liver contributes to obesity-induced insulin resistance and type 2 diabetes. Mice with diet-induced obesity (DIO mice) treated with chromogranin A peptide catestatin (CST) showed several positive results. These included decreased hepatic/plasma lipids and plasma insulin, diminished expression of gluconeogenic genes, attenuated expression of proinflammatory genes, increased expression of anti-inflammatory genes in McMΦs, and inhibition of the infiltration of McMΦs resulting in improvement of insulin sensitivity. Systemic CST knockout (CST-KO) mice on normal chow diet (NCD) ate more food, gained weight, and displayed elevated blood glucose and insulin levels. Supplementation of CST normalized glucose and insulin levels. To verify that the CST deficiency caused macrophages to be very proinflammatory in CST-KO NCD mice and produced glucose intolerance, we tested the effects of (sorted with FACS) F4/80^{+}Ly6C^{-} cells (representing KCs) and F4/80^{-}Ly6C^{+} cells (representing McMΦs) on hepatic glucose production (HGP). Both basal HGP and glucagon-induced HGP were markedly increased in hepatocytes cocultured with KCs and McMΦs from NCD-fed CST-KO mice, and the effect was abrogated upon pretreatment of CST-KO macrophages with CST. Thus, we provide a novel mechanism of HGP suppression through CST-mediated inhibition of macrophage infiltration and function.

The liver integrates nutrient, hormonal, and environmental signals to regulate glucose and lipid metabolism but also plays a key role as part of the immune system by secreting acute-phase proteins, complement components, cytokines, and chemokines and contains resident immune cells (1,2). In obesity, accumulation of proinflammatory lipids such as diglycerides and ceramides cause liver damage, inflammation, and hepatic insulin resistance (IR) (3–5). Macrophages (MΦs) infiltrate metabolic organs under obese conditions and contribute to low-grade inflammation that impairs insulin action, leading to the development of IR (6). The crucial role of MΦs in hepatic inflammation and IR is supported by experiments showing improved insulin sensitivity after chemical deletion or genetic impairment of MΦs (7,8).

In lean animals, insulin stimulates storage of glucose as liver glycogen and inhibits hepatic glucose production (HGP) by inhibiting glycogenolysis and gluconeogenesis. In contrast, in obesity and type 2 diabetes, the liver becomes insulin resistant, resulting in increased glycogenolysis and gluconeogenesis with a consequent increase in overall HGP. Tissue resident and recruited MΦs both contribute to the increased inflammatory state of the liver in obesity and type 2 diabetes. There are two important MΦ populations in the liver: the resident Kupffer cells (KCs) and recruited monocyte-derived MΦs (McMΦs). Obesity activates KCs to a more inflammatory or M1 state (9), which leads to migration of inflammatory monocytes (Ly6C^{+} in mice) into the liver, where they differentiate into McMΦs, exacerbating the severity of obesity-induced hepatic inflammation (10). Inflammatory activation of KCs has been implicated

[1]Department of Medicine, University of California, San Diego, La Jolla, CA
[2]California Institute of Technology, Pasadena, CA
[3]Department of Medicine, David Geffen School of Medicine, University of California, Los Angeles, Los Angeles, CA
[4]VA San Diego Healthcare System, San Diego, CA
[5]Istituto di Ricovero e Cura a Carattere Scientifico San Raffaele Scientific Institute, San Raffaele Vita-Salute University, Milan, Italy

Corresponding author: Sushil K. Mahata, smahata@ucsd.edu.

Received 5 July 2017 and accepted 28 January 2018.

This article contains Supplementary Data online at http://diabetes.diabetesjournals.org/lookup/suppl/doi:10.2337/db17-0788/-/DC1.

in both obesity-induced IR and fatty liver disease (11). In contrast, the anti-inflammatory activation of KCs results in attenuation of obesity-induced IR (12).

We have previously shown that catestatin (CST), a chromogranin A (CgA)-derived peptide ($hCgA_{352–372}$), inhibits catecholamine secretion, reduces hypertension, provides cardioprotection, promotes angiogenesis, and enhances lipid disposal (13,14) in mice. In humans, whose plasma CST levels vary from 0.33 nmol/L to 1.5 nmol/L, the levels of CST are not only diminished in the case of essential hypertension but are also diminished in normotensive individuals with a positive family history for hypertension (14). Furthermore, low conversion of CgA to CST is associated with increased mortality in patients hospitalized with acute heart failure (14), and low plasma CST levels also correlate with low plasma levels of cholesterol-rich HDL particles (15). In the current study, we investigated the role of CST on hepatic MΦ recruitment and function as well as on regulation of obesity-induced hepatic inflammation and IR.

RESEARCH DESIGN AND METHODS

Animals, Diets, and Treatments

Male wild-type (WT) and CST knockout (CST-KO) C57BL/6J mice were kept in a 12:12 h dark:light cycle. The Institutional Animal Care and Use Committee approved all procedures and animals were housed and handled in accordance with National Institutes of Health animal care guidelines.

Male mice (8 weeks of age) were fed ad libitum for 16 weeks with a high-fat diet (HFD) (D12492, 60% of calories from fat; Research Diets) to create diet-induced obesity (DIO); water was available at all times. Control mice were fed a normal chow diet (NCD) (14% of calories from fat). Chronic CST treatments (5 μg/g body wt i.p. for 15 days) were initiated after 11 weeks of HFD feeding, when weight gains practically leveled off.

Immunoassays

Total CgA (full-length CgA plus fragments), full-length CgA (CgA_{445}), and the CST fragment ($CgA_{1–385}$) were detected by sandwich ELISAs (16,17).

In Vitro Chemotaxis Assay

In vitro chemotaxis assays were performed as previously described (18).

Determination of Plasma Cytokines

Plasma cytokine concentrations were determined by a multiplex system from Quansys Biosciences (Logan, UT) as previously described (18) and V-PLEX proinflammatory panel 1 kit from Meso Scale Diagnostics (Rockville, MD).

Isolation and FACS Analysis of Liver MΦs

Liver MΦs were isolated by two-step liver collagenase digestion and fractionation on a two-step Percoll density gradient as previously described (19). Single-cell suspensions from the supernatant fraction were incubated with fluorescence-tagged antibodies against Ly6C and F4/80 and isolated using a BD FACS Aria II flow cytometer.

Coculture Assay

Primary hepatocytes were prepared from NCD-fed WT mice and cultured as previously described (19). Recruited McMΦs were sorted as $F4/80^{-}Ly6C^{+}$ and KCs as $F4/80^{+}Ly6C^{-}$. McMΦs or KCs (0.1×10^{6}) were plated for 24 h on a transwell membrane in RPMI + 10% FBS. Transwell inserts were then transferred to a plate containing cultured primary hepatocytes, creating a coculture setup where MΦs were on top of the separating membrane of the transwell and primary hepatocytes were at the bottom of the collagen-coated plate. At this step, culture medium was switched to Williams' Medium E with antibiotics and 0.2% BSA. After 24 h coculture, the HGP was measured.

Glucose Output Assay

Glucose output assay (19) was modified as follows. After removal of transwell inserts, hepatocyte cultures were washed twice with glucose-free HEPES salt bicarbonate buffer. Finally, cultures were incubated in the same HEPES salt bicarbonate buffer (0.3 mL/well) and treated with glucagon (200 ng/mL) and CST (100 nmol/L). A 3-μL aliquot of a mixture of pyruvate and lactate was added to each well to final concentrations of 5 mmol/L pyruvate and 10 mmol/L lactate. After 6 h, incubations were terminated and glucose concentrations in the media were determined by a commercially available glucose assay kit.

Real-time PCR

Total RNA from FACS-sorted MΦs was isolated with use of the RNeasy Mini Kit (Qiagen) and reverse transcribed with use of the qScript cDNA Synthesis Kit (Quantabio). cDNA samples were amplified with use of PerfeCTa SYBR Green FastMix L-ROX 1250 (Quantabio) and analyzed on an Applied Biosystems 7500 Fast Real-Time PCR system. All PCRs were normalized to *Gapdh*, and relative expression levels were determined by the $\Delta\Delta C_t$ (threshold cycle) method. Primer sequences are provided in Supplementary Table 1.

Transmission Electron Microscopy

Perfusion-fixed liver was resected, minced into pieces, and processed for electron microscopical analysis (20). Cells were identified as follows: hepatocytes have numerous mitochondria as well as plentiful rough and smooth endoplasmic reticula. KCs are exclusively located in the hepatic sinusoids and contain fewer mitochondria and rough endoplasmic reticula. Hepatic stellate cells (SCs) are perisinusoidal and contain characteristic large lipid droplets and stacked layers of extracellular collagen deposition. Recruited monocytes are small and have an increased nuclear-to-cytoplasmic ratio and after differentiation to McMΦ show phagocytic vacuoles.

Data Presentation and Statistical Analysis

Data are expressed as mean ± SEM. Statistical analyses were performed with GraphPad Prism 7 software. Data were analyzed by one-way, two-way, or three-way ANOVA followed by multiple comparison tests where appropriate. Individual pairwise comparisons were performed using

unpaired Student *t* tests. Statistical significance was defined as $P < 0.05$.

RESULTS

CST Treatment Inhibits Recruitment of McMΦs in Liver and Decreases Circulating Proinflammatory Cytokines in DIO Mice, Implicating CST as an Anti-inflammatory Peptide

DIO mice showed decreased total plasma CgA (Fig. 1*A*), full-length CgA (Fig. 1*B*), and CST fragment (Fig. 1*C*). The ratio of full-length CgA/CST fragment was increased (Fig. 1*D*), implying decreased conversion of CgA to CST in DIO mice. Hepatic cell content and structure was investigated by transmission electron microscopy (TEM) (Fig. 1*E–J*). Cell numbers were quantified from multiple sections (Fig. 1*K*). Normal liver showed abundant hepatocytes and smaller numbers of KC and SC but few monocytes (Fig. 1*F* and *G*). Livers from DIO mice showed steatosis due to excess fat storage in hepatocytes (Fig. 1*H* and *I*), which activates KCs to secrete a large variety of cytokines and chemokines, resulting in recruitment of McMΦs. In addition to hepatocyte lipid droplets, the sections from DIO livers showed marked infiltration of recruited McMΦs between the hepatocytes (Fig. 1*I*). Treatment with CST decreased steatosis in WT DIO liver (Fig. 1*J*) and inhibited infiltration of McMΦs in DIO liver (Fig. 1*J* and *K*). Consistent with the

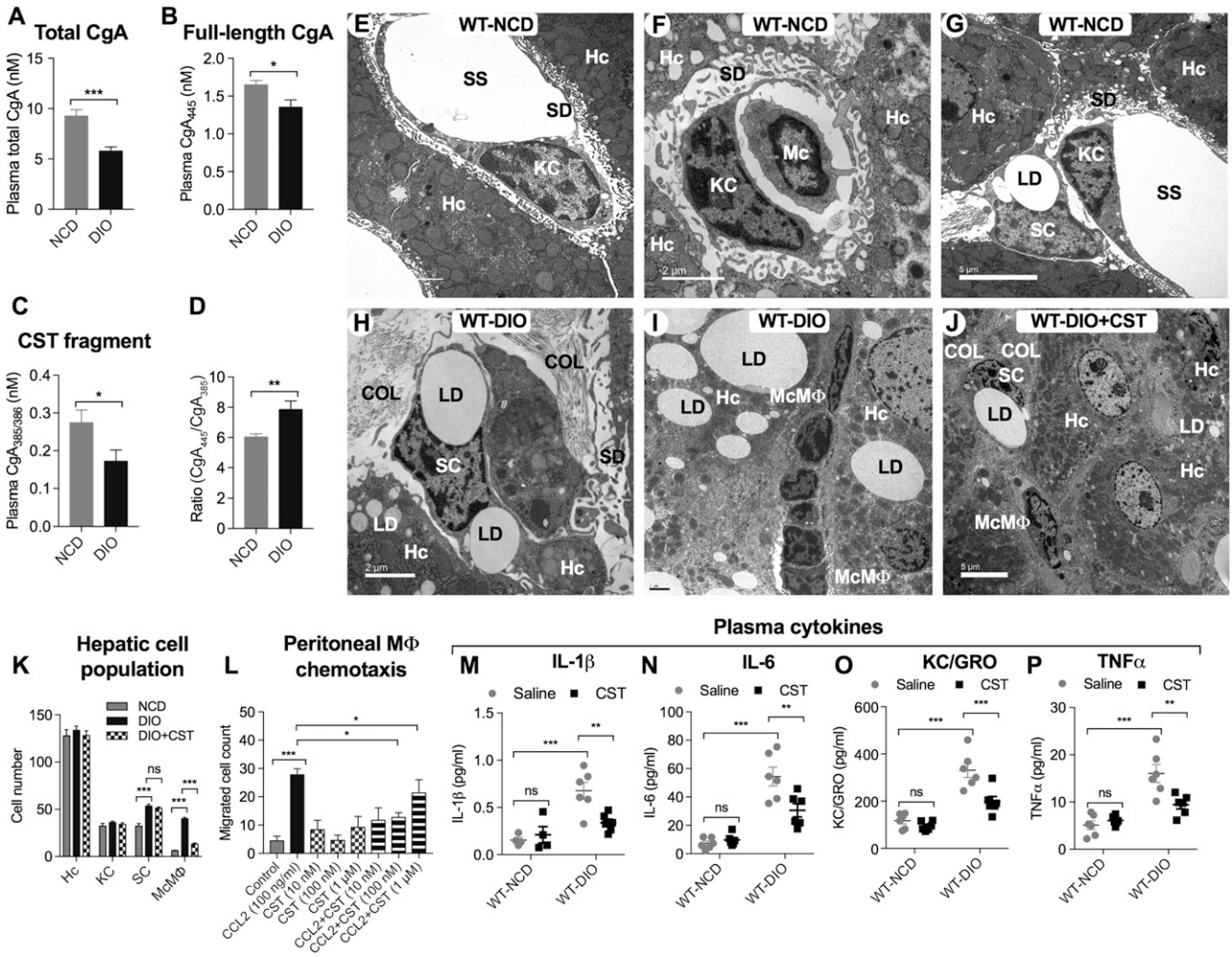

Figure 1—*A–D*: Plasma CgA and its fragments (n = 12–24). Total CgA (full-length plus processed) (*A*), full-length CgA (*B*), CST fragment (*C*), and ratio of full-length CgA and CST fragment (*D*). *E–J*: TEM photograph of liver sections (n = 4). *E*: WT NCD liver showing hepatocytes (Hc), KCs, and associated subcellular structures. *F*: WT NCD liver showing hepatocytes, monocyte (Mc), and associated subcellular structures. *G*: WT NCD liver showing hepatocytes, KCs, and SCs. *H*: WT DIO liver showing SCs. *I*: WT DIO liver showing hepatocytes, infiltrated McMΦs in the interhepatocyte space, and associated subcellular structures. *J*: WT DIO liver showing CST-induced inhibition of infiltration of McMΦs and associated subcellular structures. Scale bars: *E*, *G*, and *J* = 5 μm; *F*, *H*, and *I* = 2 μm. *K*: Morphometric analyses of parenchymal and nonparenchymal cells. Hepatocyte and KC numbers were comparable in WT NCD, WT DIO, and WT DIO+CST-treated groups. SC and McMΦ numbers were increased in WT DIO mice. Note that CST treatment of DIO mice caused significant decreases in McMΦs but exerted no effect on SCs. *L*: Chemotaxis of peritoneal MΦs (n = 5). CCL2-induced peritoneal MΦ was significantly inhibited by CST (10 and 100 nmol/L doses). *M–P*: Plasma cytokines (n = 5–8). CST inhibited inflammatory plasma cytokines. COL, collagen; LD, lipid droplet; SD, space of Disse or perisinusoidal space; SS, sinusoidal space. $^*P < 0.05$; $^{**}P < 0.01$; $^{***}P < 0.001$.

in vivo results, CCL2/MCP-1–induced chemotaxis of peritoneal MΦs in vitro was also reduced by CST treatment (Fig. 1*L*). Plasma cytokines were measured on NCD and DIO mice with and without CST treatment. The plasma levels of IL-1β, IL-6, KC/GRO, and TNF-α are all elevated in DIO mice, but CST suppresses them (Fig. 1*M–P*). CST also reduced expression of IFNγ and CCL2/MCP-1 in DIO plasma (Supplementary Fig. 1*E* and *F*) but had no effect on IL-2 or IL-5 (Supplementary Fig. 1*C* and *D*).

Liver MΦs From DIO Mice Display Altered Ultrastructural Characteristics

Morphometric analysis of FACS-purified McMΦs and KCs after TEM showed that F4/80$^-$Ly6C$^+$ McMΦs are smaller than F4/80$^+$Ly6C$^-$ KCs in mice on NCD (Fig. 2*A*, *D*, and *G*). The nuclear-to-cytoplasmic ratio is much higher in F4/80$^-$Ly6C$^+$ cells compared with F4/80$^+$Ly6C$^-$ cells (Fig. 2*A–F* and *H*). While DIO had no significant effect on nuclear-to-cytoplasmic ratio in F4/80$^+$Ly6C$^-$ KCs, the ratio was decreased in F4/80$^-$Ly6C$^+$ McMΦs, due to expansion of the cytoplasm (Fig. 2*H*). CST treatment, however, normalized the McMΦ nuclear-to-cytoplasmic ratio in DIO mice (Fig. 2*F* and *H*). DIO increased phagocytic vacuole area in both cell populations (Fig. 2*I*) but only increased phagocytic vacuole volume density in F4/80$^-$Ly6C$^+$ McMΦs (Fig. 2*J*). CST treatment caused decreased phagocytic area and volume density in both F4/80$^-$Ly6C$^+$ McMΦs and F4/80$^+$Ly6C$^-$ KCs (Fig. 2*I* and *J*).

CST Treatment Reduces Hepatic Lipid Content and Improved Lipid Profile in DIO Mice

Consistent with the reduced steatosis (Supplementary Fig. 2*A–F*), CST reduced liver weight in DIO mice (Supplementary Fig. 3*F*) and reduced both hepatic and plasma

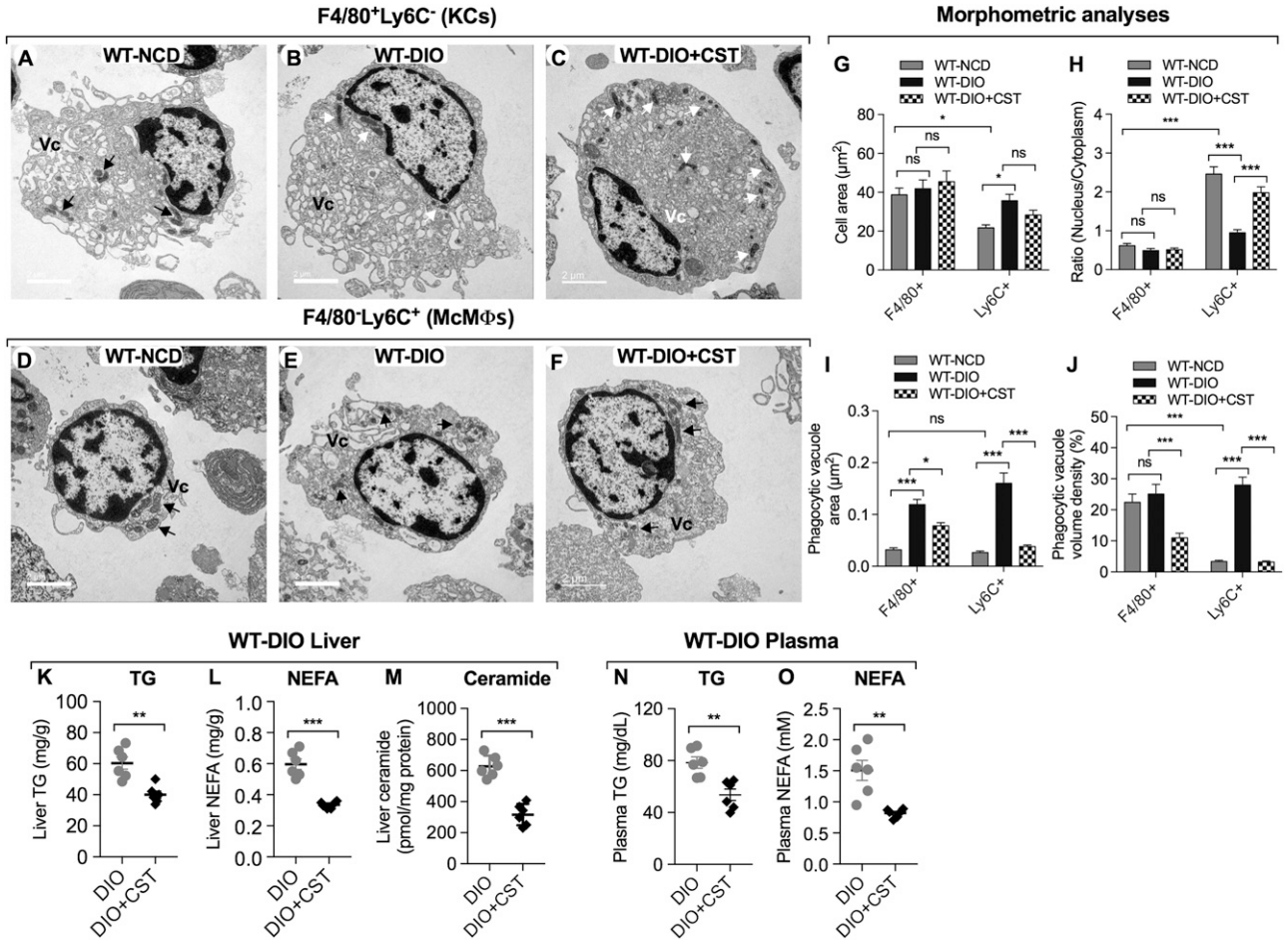

Figure 2—*A–F*: Ultrastructural changes in FACS-sorted MΦs. A representation of F4/80$^+$Ly6C$^-$ cells in NCD (*A*), DIO (*B*), and DIO+CST-treated (*C*) mice and a representation of F4/80$^-$Ly6C$^+$ cells in NCD (*D*), DIO (*E*), and DIO+CST-treated (*F*) mice. Scale bars: *A–F* = 2 μm. *G*: Cell area. F4/80$^-$Ly6C$^+$ cells are smaller than F4/80$^+$Ly6C$^-$ cells. Note that DIO caused an increase in F4/80$^-$Ly6C$^+$ cell area. *H*: Nuclear-to-cytoplasmic ratio. The ratio is much higher in F4/80$^-$Ly6C$^+$ cells compared with F4/80$^+$Ly6C$^-$ cells. Note that DIO caused a decrease in this ratio, which was increased again after CST treatment. *I*: Phagocytic vacuole area: note increased phagocytic vacuole areas in both DIO F4/80$^+$Ly6C$^-$ and F4/80$^-$Ly6C$^+$ cells that were decreased by CST. *J*: Phagocytic vacuole volume density. Note increased phagocytic volume density in F4/80$^-$Ly6C$^+$ cells. CST treatment decreased volume density in DIO F4/80$^+$Ly6C$^-$ and F4/80$^-$Ly6C$^+$ cells. *K–O*: Tissue and plasma lipids (n = 6). Treatment of WT DIO mice with CST resulted in decrease of TG (*K*), NEFAs (*L*), and ceramide (*M*) in liver as well as TG (*N*) and NEFA (*O*) in plasma. Mitochondria are shown by black and white arrows. Vc, phagocytic vacuole. *$P < 0.05$; **$P < 0.01$; ***$P < 0.001$.

triglyceride (TG) and nonesterified fatty acid (NEFA) levels (Fig. 2*K*, *L*, *N*, and *O*) as well as collagen accumulation (Supplementary Fig. 1*A* and *B*). CST also suppressed the level of proinflammatory ceramides in DIO liver (Fig. 2*M*).

CST Treatment Inhibits Recruitment of F4/80$^-$Ly6C$^+$ Monocytes/MΦs in DIO Liver and Modulates the Expression of Pro- and Anti-inflammatory Genes

FACS analyses revealed that CST caused a marked reduction in infiltration of F4/80$^-$Ly6C$^+$ McMΦs in DIO liver (Fig. 3*A* and *B*), consistent with the morphometric analysis (Fig. 1*K*). The expression of MΦ markers and cytokines was measured in the purified F4/80$^-$Ly6C$^+$ McMΦs and F4/80$^+$Ly6C$^-$ KCs (Fig. 3*C* and *D*). F4/80$^-$Ly6C$^+$ McMΦs showed low expression of *Emr1/F4/80* and increased expression of *Tnf*, *Ifng*, *Nos2*, and *Ccl2/Mcp1* genes compared with F4/80$^+$Ly6C$^-$ KCs but comparable expression of *Itgam/CD11b* and *Itgax/CD11c* genes (Fig. 3*C* and *D*). Treatment of NCD mice with CST did not alter expression of any MΦ or cytokine gene (Supplementary Fig. 3), but treatment of DIO mice resulted in marked suppression of proinflammatory gene expression in both F4/80$^-$Ly6C$^+$ McMΦs and F4/80$^+$Ly6C$^-$ KCs (Fig. 3*E* and *G*). Interestingly, CST treatment resulted in increased expression of the anti-inflammatory genes *Il10*, *Il4*, *Arg1*, *Clec10a/Cd301*, and *Mrc1/Cd206* in F4/80$^-$Ly6C$^+$ McMΦs but only *Il10* and *Clec10a/Cd301* in F4/80$^+$Ly6C$^-$ KCs (Fig. 3*F* and *H*). Similar anti-inflammatory effects were seen in vitro. CST treatment (100 nmol/L for 24 h) of FACS-sorted F4/80$^+$Ly6C$^-$ and F4/80$^-$Ly6C$^+$ cells decreased expression of proinflammatory genes in both cell populations (Fig. 3*I* and *K*) and increased expression of anti-inflammatory genes *Il10*, *Il4*, *Arg1*, *Clec10a/Cd301*, *Mgl2*, *Clec7a*, and *Mrc1/Cd206* in F4/80$^-$Ly6C$^+$ McMΦs cells and *Il10*, *Clec10a/Cd301*, and *Mrc1/Cd206* in F4/80$^+$Ly6C$^-$ KCs (Fig. 3*J* and *L*).

CST Treatment Improves Glucose and Insulin Tolerance

CST-KO mice are glucose and insulin intolerant on NCD, and treatment with CST normalized these parameters but did not change glucose tolerance or insulin sensitivity in WT mice on NCD (Fig. 4*A–D*). In contrast, CST treatment improved glucose tolerance and insulin sensitivity in both obese WT and CST-KO mice (Fig. 4*E–H*). The improvements were associated with a decrease in the expression of gluconeogenic genes, including glucose-6-phosphatase (*G6pc*) (Fig. 4*I*) and phosphoenolpyruvate-carboxykinase (*Pck1*) (Fig. 4*J*) as well as lower plasma insulin levels (Fig. 4*K* and *L*). As expected, HFD feeding caused increased body weight (BW) and food intake in WT and CST-KO mice. CST treatment did not decrease food intake for either genotype on either NCD or HFD, but it reduced BW in CST-KO on either diet while having no effect in WT mice (Supplementary Fig. 4*A–D*). Of note, CST treatment reduced liver weight in both obese WT and obese CST-KO mice, consistent with the reduced steatosis, and also in CST-KO on NCD (Supplementary Fig. 4*E* and *F*). CST did not reduce epididymal adipose tissue (eWAT) weight in either obese WT or obese CST-KO mice but reduced eWAT in CST-KO mice on NCD (Supplementary Fig. 4*E–H*).

CST Prevents MΦ-Induced HGP

To test whether MΦs are required for the improvement in glucose and insulin sensitivity after CST treatment, we depleted antigen-presenting cells with clodronate. Clodronate alone partially improves glucose and insulin tolerance in WT DIO mice (Fig. 4*M* and *N*), but importantly, it completely eliminates the effect of CST. To test whether CST could have a direct effect on HGP, we cultured hepatocytes from lean WT mice and treated them with glucagon to stimulate glucose production, with or without cotreatment with insulin or CST. Both insulin and CST suppressed glucagon-induced glucose production (Fig. 4*O*). We then cocultured lean WT hepatocytes with FACS-purified F4/80$^+$Ly6C$^-$ KCs or F4/80$^-$Ly6C$^+$ McMΦs isolated from lean WT or CST-KO mice. Cultures using MΦs from CST-KO mice were also treated with CST. Both F4/80$^+$Ly6C$^-$ KCs and F4/80$^-$Ly6C$^+$ McMΦs from the CST-KO mice had a dramatic increase in basal and glucagon-stimulated glucose production, which was completely reversed by CST treatment (Fig. 4*P* and *Q*). Since both types of MΦ populations had stimulated glucose production, this suggests that KCs are also activated in CST-KO mice.

DISCUSSION

In this study, we showed that CST is reduced in obesity and acts as an anti-inflammatory peptide to reduce obesity-induced hepatic IR. Treatment of DIO mice with CST resulted in decreased proinflammatory gene expression in KCs and McMΦs, as well as decreased circulating inflammatory cytokines and improved insulin sensitivity. At the cellular level, we showed a dramatic increase in glucose production from hepatocytes cocultured with KCs or McMΦs from CST-KO mice that was completely abolished by coincubation with CST. This indicates that the improved whole-body glucose and insulin sensitivity may be mediated, at least in part, by the anti-inflammatory effects of CST on hepatic KCs and MΦs. As well as having direct anti-inflammatory effects, CST treatment also resulted in decreased MΦ migration to the liver, suggesting that CST regulated both MΦ recruitment and activation. This was further supported by the elimination of the protective effect of CST in clodronate-treated, MΦ-depleted DIO mice. Our results are consistent with those of Morinaga et al. (19), who found that culture medium from recruited hepatic MΦs directly stimulated hepatic glucose output.

Our ultrastructural findings revealed that recruited McMΦs are smaller than KCs in NCD-fed mice, as previously reported (19). Previous studies have characterized distinct subpopulations of hepatic MΦs in DIO mice using a combination of in vivo MΦ tracking methodologies and adoptive transfer techniques (19). These studies revealed ~sixfold higher number of recruited hepatic MΦs (McMΦs) in DIO mice compared with lean mice (19), while the number of KCs was comparable between the two

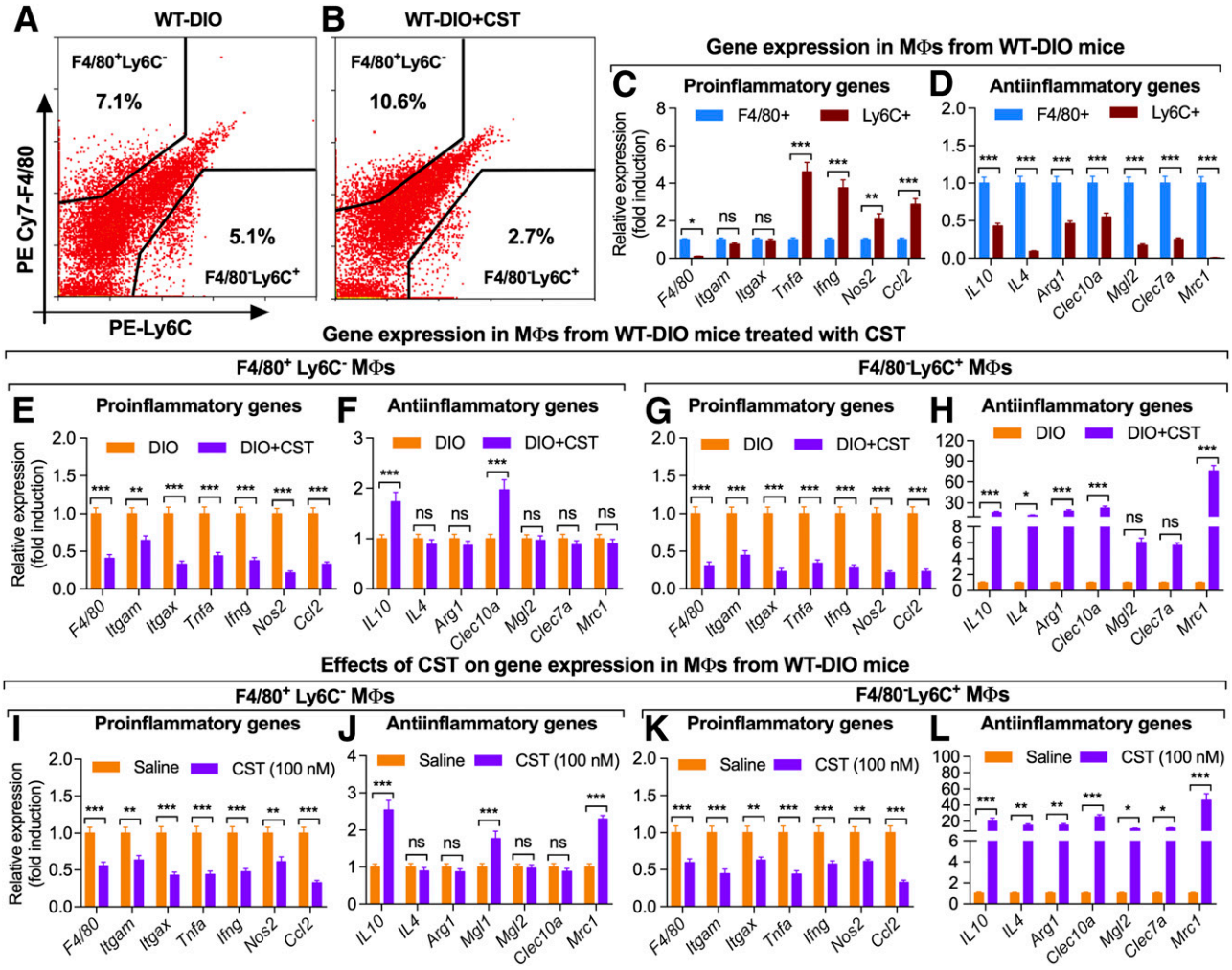

Figure 3—FACS-sorted MΦs (n = 6). CST caused dramatic inhibition of infiltration of Ly6C$^+$ cells in DIO liver (*A* and *B*). Data were analyzed by two-way ANOVA followed by Tukey multiple comparison test. Interaction, $P < 0.001$; genes, $P < 0.001$; MΦs, $P < 0.001$. PE, phycoerythrin. Gene expression in MΦs from DIO liver (n = 6): note increased expression of proinflammatory and decreased expression of anti-inflammatory genes in Ly6C$^+$ cells compared with F4/80$^+$ cells (*C* and *D*). Data were analyzed by two-way ANOVA followed by Tukey multiple comparison test. Interaction, $P < 0.001$; genes, $P < 0.001$; MΦs, $P < 0.001$. *E–H*: Gene expression in MΦs from DIO mice treated with CST (n = 6): *E*: Proinflammatory gene expression in F4/80$^+$Ly6C$^-$ cells. Data were analyzed by two-way ANOVA followed by Tukey multiple comparison test. Interaction, ns; genes, ns; treatment, $P < 0.001$. *F*: Anti-inflammatory gene expression in F4/80$^+$Ly6C$^-$ cells. Data were analyzed by two-way ANOVA followed by Tukey multiple comparison test. Interaction, $P < 0.001$; genes, $P < 0.001$; treatment, $P < 0.01$. *G*: Proinflammatory gene expression in F4/80$^-$Ly6C$^+$ cells. Data were analyzed by two-way ANOVA followed by Tukey multiple comparison test. Interaction, ns; genes, ns; treatment, $P < 0.001$. *H*: Anti-inflammatory gene expression in F4/80$^-$Ly6C$^+$ cells. Data were analyzed by two-way ANOVA followed by Tukey multiple comparison test. Interaction, $P < 0.001$; genes, $P < 0.001$; treatment, $P < 0.001$. Note that CST decreased expression of proinflammatory genes in both F4/80$^+$ and Ly6C$^+$ cells (*E* and *G*). In contrast, CST increased expression of only *IL10* and *Clec10a/Cd301* in F4/80$^+$ cells and all anti-inflammatory genes tested in Ly6C$^+$ cells (*F* and *H*). *I–L:* Direct effects of CST on expression of genes in cultured MΦs (n = 6). *I*: Proinflammatory gene expression in F4/80$^+$Ly6C$^-$ cells. Data were analyzed by two-way ANOVA followed by Tukey multiple comparison test. Interaction, ns; genes, ns; treatment, $P < 0.001$. *J*: Anti-inflammatory gene expression in F4/80$^+$Ly6C$^-$ cells. Data were analyzed by two-way ANOVA followed by Tukey multiple comparison test. Interaction, $P < 0.001$; genes, $P < 0.001$; treatment, $P < 0.01$. *K*: Proinflammatory gene expression in F4/80$^-$Ly6C$^+$ cells. Data were analyzed by two-way ANOVA followed by Tukey multiple comparison test. Interaction, ns; genes, ns; treatment, $P < 0.001$. *L*: Anti-inflammatory gene expression in F4/80$^-$Ly6C$^+$ cells. Data were analyzed by two-way ANOVA followed by Tukey multiple comparison test. Interaction, $P < 0.001$; genes, $P < 0.001$; treatment, $P < 0.001$. The effects of CST on cultured MΦs are similar to the in vivo effects except that CST increased expression of *Mrc1* in addition to IL10 and Mrc1 in F4/80$^+$ cells (*I–L*). *$P < 0.05$; **$P < 0.01$; ***$P < 0.001$.

groups. Our ultrastructural study also revealed for the first time a prefibrotic condition in liver at later stages of obesity in mice, with extracellular collagen deposition around SCs, suggesting their activation.

CST has previously been linked to inflammatory signaling (21). In a mouse model of colitis caused by dextran sulfate ingestion, CST not only attenuated the severity of inflammation but also reduced the production of proinflammatory mediators in the gut (21). In addition, CST caused a significant downregulation of myeloperoxidase activity, serum CRP, and proinflammatory cytokines, indicating CST as a gut anti-inflammatory peptide. CST has also

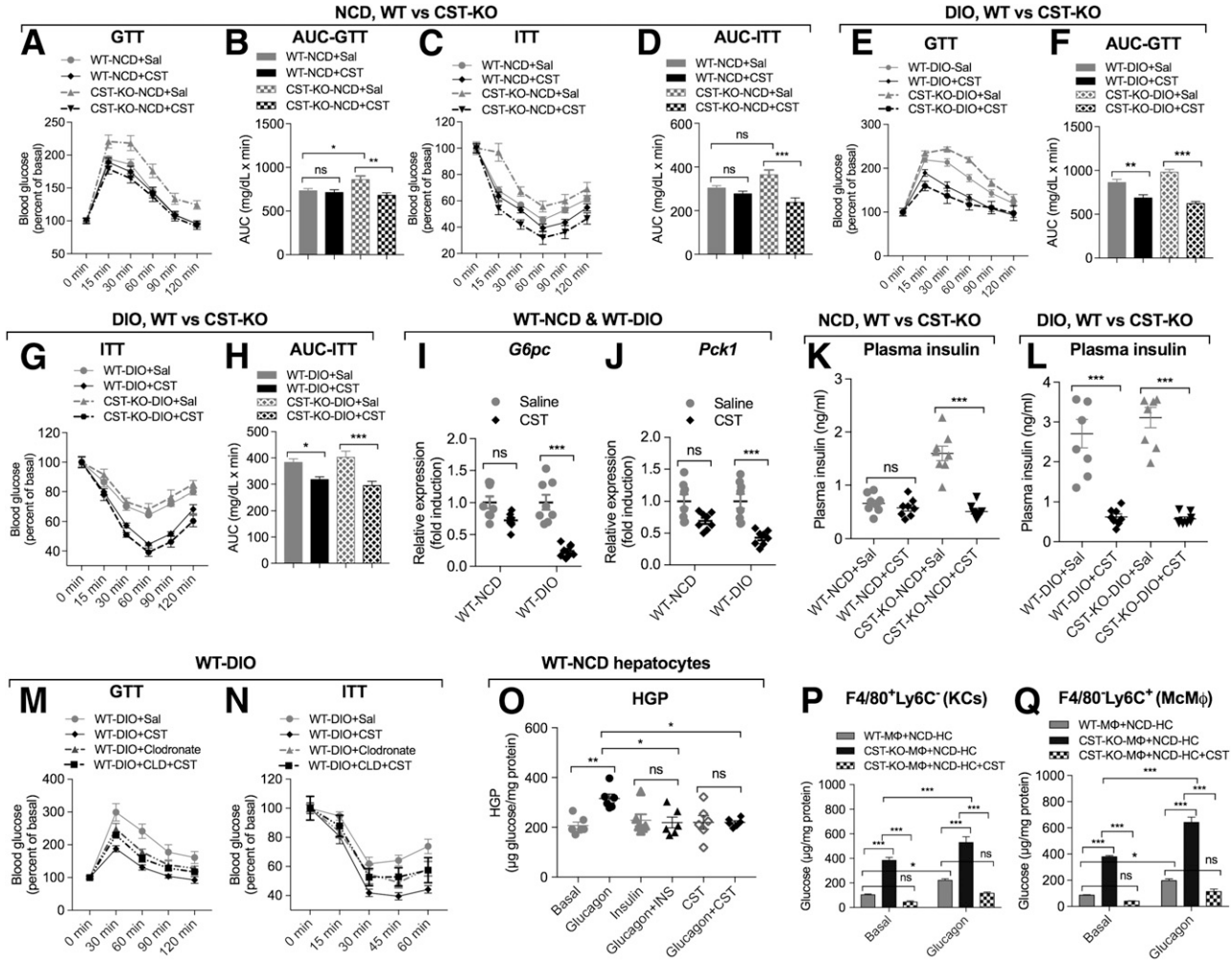

Figure 4—*A–D*: CST improves glucose tolerance and insulin sensitivity in CST-KO NCD mice. Glucose tolerance test (GTT) (n = 10) on mice fasting for 10 h (*A*) and the corresponding area under the curve (AUC) (*B*). Data were analyzed by three-way ANOVA. Time, $P < 0.001$; treatment, $P < 0.01$; genotype, $P < 0.001$; time × treatment, ns; time × genotype, $P < 0.05$; treatment × genotype: $P < 0.001$; time × treatment × genotype: ns. Insulin tolerance test (ITT) (n = 8) on mice fasting for 10 h (*C*) and the corresponding area under the curve (*D*). Data were analyzed by three-way ANOVA. Time, $P < 0.001$; treatment, ns; genotype, $P < 0.001$; time × treatment, ns; time × genotype, $P < 0.01$; treatment × genotype, $P < 0.001$; time × treatment × genotype, $P < 0.05$. *E–H*: CST improves glucose tolerance and insulin sensitivity in both WT DIO and CST-KO DIO mice (n = 9); phenotypes of NCD-fed CST-KO mice. Glucose tolerance test (n = 8) on mice fasting for 10 h (*E*) the corresponding area under the curve (*F*). Data were analyzed by three-way ANOVA. Time, $P < 0.001$; treatment, $P < 0.05$; genotype, $P < 0.001$; time × treatment, ns; time × genotype, $P < 0.001$; treatment × genotype, $P < 0.001$; time × treatment × genotype, $P < 0.01$. Insulin tolerance test (n = 8) on mice fasting for 10 h (*G*) and the corresponding area under the curve (*H*). Data were analyzed by three-way ANOVA. Time, $P < 0.001$; treatment, ns; genotype, $P < 0.001$; time × treatment, ns; time × genotype, $P < 0.01$; treatment × genotype, $P < 0.001$; time × treatment × genotype, ns. *I* and *J*: CST decreases expression of gluconeogenic genes in DIO liver (after 10 h fasting) (n = 8). Expression of *G6pc* gene (*I*) and *Pck1* gene (*J*). *K* and *L*: CST decreases plasma insulin in CST-KO NCD, WT DIO, and CST-KO DIO mice (after 10 h fasting). Plasma insulin (n = 8) in WT NCD and CST-KO NCD mice (*K*) as well as in WT DIO and CST-KO DIO mice (*L*). *M* and *N*: Depletion of MΦs abolishes CST-induced improvement in glucose tolerance and insulin sensitivity in WT DIO mice (n = 6). Glucose tolerance test (*M*) and insulin tolerance test (*N*). *O*: HGP, n = 6. CST decreases glucagon-induced HGP in WT-NCD hepatocytes. *P* and *Q*: HGP by MΦs from NCD-fed CST-KO mice (n = 4). F4/80$^+$ MΦs (*P*) and Ly6C$^+$ MΦs (*Q*). Note the dramatic increase in basal glucose production in hepatocytes (HC) cocultured with both F4/80$^+$ and Ly6C$^+$ cells from CST-KO mice. Glucagon caused an even further increase in glucose production in both cell types. Increased glucose production was completely inhibited when hepatocytes were cocultured with CST-treated MΦs and incubated with glucagon. INS, insulin; Sal, saline. *$P < 0.05$; **$P < 0.01$; ***$P < 0.001$.

been shown to enter polymorphonuclear neutrophils and activate the release of several anti-inflammatory proteins involved in innate immunity including lactotransferrin (22,23). The present studies provide a novel pathway for suppression of HGP through CST-mediated inhibition of MΦ infiltration and function. It is reasonable to conclude that paracrine factors released locally from MΦs may alter hepatocyte function and that CST may inhibit the production of such factors. In support of this idea, conditioned medium from coculture of hepatocytes and MΦs was found to contain matrix metalloproteinase (MMP)-9 (24) and lymphocyte-activating factor (25) that may induce proinflammatory gene expression in hepatocytes. It should be noted that the anti-inflammatory effect of CST in obese

mice is not due to decreased adiposity, as food intake and eWAT weights were not reduced in obese mice by CST treatment. In CST-KO DIO mice, absence of CST increases food intake and BW, which was normalized after CST treatment, so endogenous CST may help maintain BW by suppressing food intake and enhancing glucose tolerance, especially under conditions of nutrient excess. Furthermore, exogenous CST can compensate for the decreased level of endogenous CST in DIO, partially reverse the hepatic steatosis, and improve both glucose and insulin tolerance.

In conclusion, our work demonstrated that CST can *1*) directly suppress glucose production from hepatocytes, *2*) indirectly suppress lipid accumulation in liver, and *3*) indirectly suppress MΦ-mediated inflammation in obese mice. The net results are improved glucose tolerance and insulin sensitivity in obese mice.

Acknowledgments. TEM was conducted at the Cellular & Molecular Medicine Electron Microscopy Core Facility at University of California, San Diego.

Funding. W.Y. was supported by the American Heart Association (16POST31350039) and the National Natural Science Foundation of China (81600610). The Noland Scholarship from the California Institute of Technology supported S.M. This research was supported mainly by S.K.M.'s personal fund and partly by a grant from the Department of Veterans Affairs (VA Merit Review [I01BX002709 to N.J.G.W. and I01BX000323 to S.K.M.]) and a Senior Research Career Scientist award to N.J.G.W.

Duality of Interest. No potential conflicts of interest relevant to this article were reported.

Author Contributions. W.Y., S.M., G.K.B., Z.Z., J.W., J.V., R.M., N.-W.C., A.C., and S.K.M. researched data. W.Y., G.K.B., and S.K.M. wrote the manuscript. N.J.G.W. participated in discussion and reviewed and edited the manuscript. S.K.M. conceived and designed the study, researched and analyzed data, and made the graphics. W.Y., G.K.B., and S.K.M. are the guarantors of this work and, as such, had full access to all the data in the study and take responsibility for the integrity of the data and the accuracy of the data analysis.

References

1. Crispe IN. The liver as a lymphoid organ. Annu Rev Immunol 2009;27:147–163
2. Nemeth E, Baird AW, O'Farrelly C. Microanatomy of the liver immune system. Semin Immunopathol 2009;31:333–343
3. Samuel VT, Shulman GI. Mechanisms for insulin resistance: common threads and missing links. Cell 2012;148:852–871
4. Hotamisligil GS, Shargill NS, Spiegelman BM. Adipose expression of tumor necrosis factor-alpha: direct role in obesity-linked insulin resistance. Science 1993;259:87–91
5. Hotamisligil GS, Peraldi P, Budavari A, Ellis R, White MF, Spiegelman BM. IRS-1-mediated inhibition of insulin receptor tyrosine kinase activity in TNF-alpha- and obesity-induced insulin resistance. Science 1996;271:665–668
6. Lumeng CN, Saltiel AR. Inflammatory links between obesity and metabolic disease. J Clin Invest 2011;121:2111–2117
7. Huang W, Metlakunta A, Dedousis N, et al. Depletion of liver Kupffer cells prevents the development of diet-induced hepatic steatosis and insulin resistance. Diabetes 2010;59:347–357
8. Jia L, Vianna CR, Fukuda M, et al. Hepatocyte Toll-like receptor 4 regulates obesity-induced inflammation and insulin resistance. Nat Commun 2014;5:3878
9. Jager J, Aparicio-Vergara M, Aouadi M. Liver innate immune cells and insulin resistance: the multiple facets of Kupffer cells. J Intern Med 2016;280:209–220
10. Gordon S, Taylor PR. Monocyte and macrophage heterogeneity. Nat Rev Immunol 2005;5:953–964
11. Krenkel O, Tacke F. Liver macrophages in tissue homeostasis and disease. Nat Rev Immunol 2017;17:306–321
12. Ju C, Tacke F. Hepatic macrophages in homeostasis and liver diseases: from pathogenesis to novel therapeutic strategies. Cell Mol Immunol 2016;13:316–327
13. Mahata SK, Mahata M, Fung MM, O'Connor DT. Catestatin: a multifunctional peptide from chromogranin A. Regul Pept 2010;162:33–43
14. Mahata SK, Kiranmayi M, Mahapatra NR. Catestatin: a master regulator of cardiovascular functions. Curr Med Chem. 24 April 2017 [Epub ahead of print]. DOI: 10.2174/0929867324666170425100416
15. Durakoğlugil ME, Ayaz T, Kocaman SA, et al. The relationship of plasma catestatin concentrations with metabolic and vascular parameters in untreated hypertensive patients: Influence on high-density lipoprotein cholesterol. Anatol J Cardiol 2015;15:577–585
16. Crippa L, Bianco M, Colombo B, et al. A new chromogranin A-dependent angiogenic switch activated by thrombin. Blood 2013;121:392–402
17. Bianco M, Gasparri AM, Colombo B, et al. Chromogranin A is preferentially cleaved into proangiogenic peptides in the bone marrow of multiple myeloma patients. Cancer Res 2016;76:1781–1791
18. Li P, Spann NJ, Kaikkonen MU, et al. NCoR repression of LXRs restricts macrophage biosynthesis of insulin-sensitizing omega 3 fatty acids. Cell 2013;155:200–214
19. Morinaga H, Mayoral R, Heinrichsdorff J, et al. Characterization of distinct subpopulations of hepatic macrophages in HFD/obese mice. Diabetes 2015;64:1120–1130
20. Pasqua T, Mahata S, Bandyopadhyay GK, et al. Impact of chromogranin A deficiency on catecholamine storage, catecholamine granule morphology and chromaffin cell energy metabolism in vivo. Cell Tissue Res 2016;363:693–712
21. Rabbi MF, Labis B, Metz-Boutigue MH, Bernstein CN, Ghia JE. Catestatin decreases macrophage function in two mouse models of experimental colitis. Biochem Pharmacol 2014;89:386–398
22. Zhang D, Shooshtarizadeh P, Laventie BJ, et al. Two chromogranin a-derived peptides induce calcium entry in human neutrophils by calmodulin-regulated calcium independent phospholipase A2. PLoS One 2009;4:e4501
23. Valenti P, Frioni A, Rossi A, et al. Aerosolized bovine lactoferrin reduces neutrophils and pro-inflammatory cytokines in mouse models of Pseudomonas aeruginosa lung infections. Biochem Cell Biol 2017;95:41–47
24. Melino M, Gadd VL, Walker GV, et al. Macrophage secretory products induce an inflammatory phenotype in hepatocytes. World J Gastroenterol 2012;18:1732–1744
25. Keller GA, West MA, Cerra FB, Simmons RL. Macrophage-mediated modulation of hepatocyte protein synthesis. Effect of dexamethasone. Arch Surg 1986;121:1199–1205